AIAA JOURNAL
Vol. 34, No. 3, March 1996

Tunable Diode Laser Measurements on Nitric Oxide in a Hypersonic Wind Tunnel

A. Mohamed,* B. Rosier,† D. Henry,‡ and Y. Louvet§
ONERA, Chatillon 92322, France
and
P. L. Varghese¶
University of Texas at Austin, Austin, Texas 78712-1085

A tunable infrared diode laser was used in the F4 high-enthalpy hypersonic wind tunnel at ONERA to make line-of-sight measurements on nitric oxide (NO). The NO is generated in the arc chamber and remains frozen in the hypersonic flow. We report the results of a medium enthalpy run. The R (14.5), $\Omega = \frac{3}{2}$ doublet was recorded simultaneously in two views: one normal to the flow and the other biased at 63-deg to the flow axis. Spectra were recorded at 2 ms intervals during a tunnel run, and 30 sets of spectra were analyzed by a least-squares fitting procedure. The mean of the velocity measurements inferred from the Doppler shift of the doublet was 2740 m/s (±5%). The velocity decayed about 10% over 60 ms. The temperature and NO column density determined by the least-squares fits were subject to much larger uncertainties. The static temperature of the freestream is estimated to be 168 K (±35%). The median inferred NO column density of 4×10^{17} molecule/cm^2 corresponds to an NO number density of order 5×10^{15} molecules/cm^3 in the freestream.

Introduction

THE F4 wind tunnel is an arc-driven high-enthalpy facility located at ONERA's Le Fauga-Mauzac test center, designed to simulate the conditions representative of Hermes re-entry. Kinetic energy stored in a 15-ton flywheel rotating at speeds up to 6000 rpm is deposited via a dc arc into the gas in the arc chamber. The gas may be either pure nitrogen or synthetic air (20% oxygen and 80% nitrogen) at pressures up to 750 bar. At the end of the arc discharge a plug in the hypersonic nozzle throat is expelled, starting the flow into the test chamber that is evacuated to a pressure below 20 Pa. Useful flow times are less than 20 ms. Further details of the facility are given in Refs. 1 and 2. The experiments described in this work were conducted using a nozzle with throat diameter of 10 mm, length of 3.20 m, and exit diameter of 670 mm. Nominal conditions in the arc chamber were stagnation pressure of 750 bar and reduced stagnation enthalpy $H_0/RT_a = 35$ ($R = 288.7$ J/kg-K and $T_a = 273$ K). The F4 facility is being used to generate benchmark data for validation of computational codes.[2] Nonintrusive measurements of the freestream velocity on every run are very desirable so that experimental conditions are known accurately. Nitric oxide (NO) is produced during the arc discharge and remains frozen in the flow as it expands through the hypersonic nozzle. Hence it was decided to test the feasibility of tunable diode laser absorption of NO as a means of measuring freestream velocity, temperature, and NO concentration. These parameters would provide valuable information to test numerical models of high-speed reacting flow in the nozzle and would also provide better initial conditions for numerical modeling of the subsequent flow around models placed in the F4 test section. The narrow laser line width and continuous tunability of diode lasers provides a means of measuring Doppler shifts accurately. The rapid tuning capability enables one to obtain data with good temporal resolution during the limited run times.

Presented as Paper 95-0428 at the AIAA 33rd Aerospace Sciences Meeting, Reno, NV, Jan. 9–12, 1995; received Feb. 17, 1995; revision received Aug. 7, 1995; accepted for publication Aug. 8, 1995.

*Research Scientist, Laser and Optical Diagnostics Division.
†Deputy Division Chief, Optical Signature Division.
‡Technician, Optical Signature Division.
§Research Scientist, Optical Signature Division.
¶Professor, Department of Aerospace Engineering and Engineering Mechanics. Senior Member AIAA.

Theory

The theory of tunable diode laser absorption and the infrared spectrum of NO are well known.[3,4] We only present a brief summary of the equations used to analyze the experimental data. The $1 \leftarrow 0$ fundamental of NO is centered near 1875 cm^{-1}. Transitions from states with total angular momentum $\Omega = \frac{3}{2}$ and $\frac{1}{2}$ are observed, and each transition consists of a closely spaced doublet arising from Λ-doubling (lower frequency component labeled e and higher frequency component labeled f). The experiments described here were performed on the $R(14.5)$, $\Omega = \frac{3}{2}$ doublet of the $1 \leftarrow 0$ fundamental centered at 1924.457 cm^{-1}. It should be noted that the choice of this transition was dictated in part by the operating characteristics of the diode laser available. A stable operating point had to be found that could be tuned continuously over a spectral line with significant absorption at the conditions of interest, but which would not attenuate the laser beam completely. Although this spectral transition is not necessarily optimal for these experiments, numerical simulations of boundary-layer effects show that it gives acceptable results. The spacing of the chosen doublet is 2.808×10^{-3} cm^{-1} and the $1/e$-Doppler halfwidth of either component is 2.138×10^{-3} cm^{-1} at 200 K. The doublet is unresolved at Doppler limited resolution and appears as a single line at the experimental conditions. However, the Λ-splitting must be accounted for when fitting experimental records if temperature is to be estimated.

In an absorption experiment the transmissivity τ at any frequency ν is given by

$$\tau(\nu) = \frac{I(\nu)}{I^0(\nu)} = \exp\left(-\int_0^L \mathrm{d}z\, \alpha(z;\nu)\right)$$

$$= \exp\left[-\int_0^L \mathrm{d}z\, n_{\mathrm{NO}} \sum_j S_j \phi_j(\nu - \nu_{0j} - \Delta\nu_V)\right] \qquad (1)$$

Here $I(\nu)$ is the transmitted intensity, $I^0(\nu)$ is the incident intensity, and $\alpha(z;\nu)$ is the absorption coefficient—a function of position z along the optical path. The number density of absorbing molecules is n_{NO}, S_j is the integrated intensity of transition j centered at ν_{0j} in a rest frame, and ϕ_j is the lineshape function. The equation $\Delta\nu_V = \nu_0 V \cos\theta/c$ is the Doppler shift due to bulk gas velocity V, where θ is the angle between the laser beam and the flow velocity, and c is the speed of light.

Each component of the doublet was assumed to be described by a Voigt profile

$$\phi(\nu) = \frac{1}{\sqrt{\pi}\Delta\nu_D} V(x, y) \tag{2}$$

where the $1/e$-Doppler halfwidth due to thermal motion is given by

$$\Delta\nu_D = 4.30 \times 10^{-7}\sqrt{T/m_{NO}}\,\nu_0 \tag{3}$$

with $T[K]$, and $m_{NO} = 30$ amu.

The factor of $\sqrt{\pi}$ arises because the standardized Voigt function used in the numerical computations is normalized to π, whereas the line shape function must be normalized to unity. The normalized frequency separation from line center x and normalized collision broadening parameter y are given by

$$\begin{aligned} x &= (\nu - \nu_{0j} - \Delta\nu_V)/\Delta\nu_D \\ y &= \Delta\nu_C/\Delta\nu_D \end{aligned} \tag{4}$$

where $\Delta\nu_C$ is the collision half-width. The Doppler shift and Doppler broadening of the two components of the doublet are the same because the difference in line center frequencies is negligible. The collision half-widths of the two components are also assumed to be identical under similar conditions. Pressure shifts in line center position are not explicitly accounted for in the analysis. They do not influence the velocity calculation because the Doppler shift is measured by comparing spectra from two views of the same gas.

The column density of NO (concentration of NO integrated along the line of sight) can be determined from the integrated intensity of the transition S and the integral of the experimentally recorded transmissivity, provided the variation of temperature with position is known. The integrated intensity at 273.2 K, $S(T_0)$, of each component of the $R(14.5)$, $\Omega = \frac{3}{2}$ doublet was taken to be 1.47×10^{-20} cm^{-1}/(molecule/cm^2) corresponding to a fundamental band strength of 4.59×10^{-18} cm^{-1}/(molecule/cm^2). The intensity of the components at any other temperature was computed from

$$S(T) = S(T_0)\frac{Q(T_0)}{Q(T)}\exp\left[-\frac{hcE}{k}\left(\frac{1}{T} - \frac{1}{T_0}\right)\right] \times \left[\frac{1 - \exp(-hc\nu/kT)}{1 - \exp(-hc\nu/kT_0)}\right] \tag{5}$$

where the total internal partition function $Q(T)$ was computed from a rigid-rotor harmonic oscillator approximation, and E [cm^{-1}] is the energy of the lower state of the transition (725.9525 and 725.9755 cm^{-1} for the e and f components, respectively). The last factor on the right side is the correction for stimulated emission.

Experimental Procedure

Measurements were made just downstream of the nozzle exit. It is estimated that the boundary layers are about 13.5 cm thick at the nozzle exit plane, giving a core flow diameter of approximately 40 cm at this location. Figure 1 is a schematic diagram of the experimental arrangement. The nominal frequency of the cryogenically cooled lead-salt diode laser was controlled by adjusting its temperature and bias current. It was rapidly and repeatedly tuned across the absorption feature by adding a sawtooth modulation of period 2 ms to the steady bias current through the laser. The output of the laser was collimated with a concave mirror and a single laser mode was selected using a diffraction grating and slit. The mode selected was recollimated and directed to a window in the test section of the wind tunnel. A beam splitter within the test section divides the beam as shown in the sketch. The undeflected beam (A) traverses the test section normal to the flow axis and emerges through a window on the opposite side. The deflected beam (B) was turned by a mirror so as to traverse the flow at an angle of 63 deg. Beam B was then reflected by a pair of mirrors so that it leaves the test chamber through the same window as beam A. The two beams are then focused separately on mercury cadmium telluride infrared detectors cooled with liquid nitrogen. The detector signals were digitized and stored for subsequent analysis.

Before an experiment the doublet was located and the experimental conditions optimized by observing NO in a room temperature absorption cell. The laser tuning rate was calibrated before a run using a Fabry–Perot etalon with free spectral range of 0.0485 cm^{-1}. A reference trace was recorded for each view to account for laser power variations with frequency. The laser was swept across the doublet so that a data trace was recorded every 2 ms in each view. The 500 kHz analog-to-digital conversion gave 300 data points in each view on every scan. (Points corresponding to the rapid sweepback of the laser at the end of each forward sweep were discarded.) The spectral interval between successive points in each record was calculated to be 1.188×10^{-4} cm^{-1}. Although typical total run times were short (150 ms), data were acquired for 1 s. For the stagnation conditions $p_0 = 750$ bar and $H_0/RT_a = 35$, profiles exhibiting the Doppler shift were recorded for a period of 60 ms starting immediately after

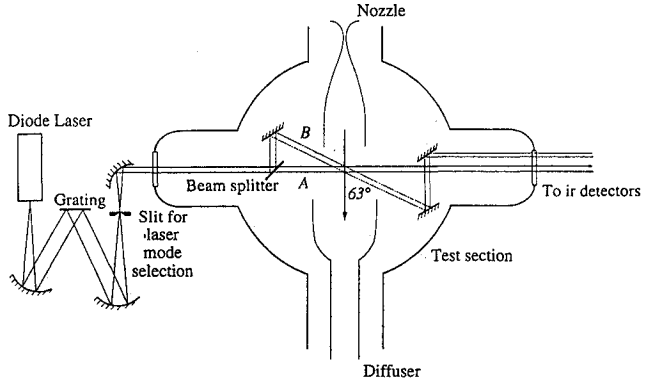

Fig. 1 Schematic diagram of the experiment.

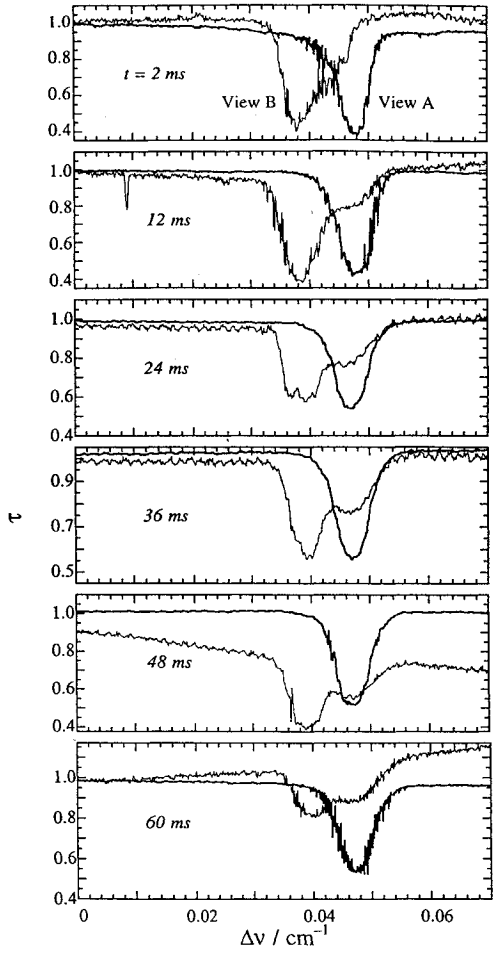

Fig. 2 Sample experimental data records. The unresolved $R(14.5)$, $\Omega = \frac{3}{2}$ doublet of NO is centered at 1924.457 cm^{-1} in the rest frame.

the plug in the nozzle throat was expelled to start the flow in the nozzle. The transmissivity was obtained by taking the ratio of each data trace with a corresponding reference trace recorded before the experiment. Significant baseline slopes and offsets of the order of several percent arising from low-frequency electrical interferences in the data channels were routinely observed and had to be corrected for during data analysis.

Figure 2 shows typical data records of transmissivity vs frequency during the course of a run. Each record shows the superposition of data obtained in unshifted channel *A* (bold line) and Doppler-shifted channel *B* (light line). The signal-to-noise ratio in channel *B* is typically poorer because the beam splitter put most of the laser power into beam *A*. The data records shown are spaced 12 ms apart (except the first pair) and correspond to $t = 2, 12, 24, 36, 48$, and 60 ms after the flow is first started in the tunnel. The first record shown corresponds to the establishment of steady state, whereas the last corresponds to the end of steady operation in the tunnel. One can see the development of a second unshifted peak in record *B* coinciding with the doublet position in record *A*. The last two records in Fig. 2 show large shifts in the nominal baseline slope and offset in channel *B* due to the effect of electrical interferences noted earlier. Simulations of absorption in the boundary layer (described later) showed that the boundary-layer absorption gives a feature that coincides with the shifted peak. Hence, the observed second peak in record *B* arises from static NO that accumulates in the test chamber during the run.

Data Analysis and Simulations

The spectrum was modeled assuming that the individual components of the doublet were described by Voigt profiles, with the same broadening parameter for each component. The doublet spacing was fixed at 2.808×10^{-3} cm^{-1} using the data of Amiot.[4] In the data analysis the influence of the boundary layers was neglected; i.e., the optical path for each view was assumed to be a combination of two homogeneous paths at different conditions: 1) the freestream and 2) the surroundings inside the low-pressure vessel exterior to the flow. This point is discussed further later.

The model spectrum was fitted to the data using a least-squares program to extract the parameters of interest. An existing program[5] that uses a Levenberg–Marquadt least-squares algorithm[6] was modified for this application. Twelve parameters were determined simultaneously from the least-squares fit: (1 and 2) Voigt broadening parameters for freestream and surroundings, (3 and 4) the temperature of NO in the freestream and surroundings (via the Doppler broadening in the Voigt profiles), (5 and 6) the integrated absorptions of the doublet in freestream and surroundings, (7 and 8) the positions of the centers of the doublet in records *A* and *B*, and (9–12) baseline offsets and slopes for each record. Provision for baseline offset and slope had to be included in the fit because they were significant in most records (see Fig. 2). The line shape parameters were constrained to be the same for the two records, the only differences being the Doppler shift (for the freestream segment of the path) and fixed geometric factors in the integrated absorptions arising from different optical paths. These factors were $1.122 = 1/\sin 63$ deg for the freestream and 1.7 for the chamber. The doublet absorption due to the surroundings in record *B* is assumed to be centered at the same position as the doublet in record *A*. The Doppler shift and hence the velocity of the jet were determined from the difference in the positions of the doublet centers in the two records. When there was no detectable unshifted absorption in record *B* (very early times), the data were analyzed assuming a single homogenous optical path. This reduces the number of fitted parameters to nine.

The fitting program was tested against synthetic data generated with known parameters to ensure that it operated as expected. An example of a fit to synthesized data records is given next. The present least-squares program is not foolproof but generally gives good fits even with noisy data provided the initial guesses are reasonable. The simulations showed that if the initial guesses were too far off, the fitting procedure failed completely. A strategy other than least squares would be more stable for fits with 9–12 free parameters. We plan to investigate this in the future. The Doppler shift is insensitive to most fitting uncertainties and hence velocity is reliably inferred.

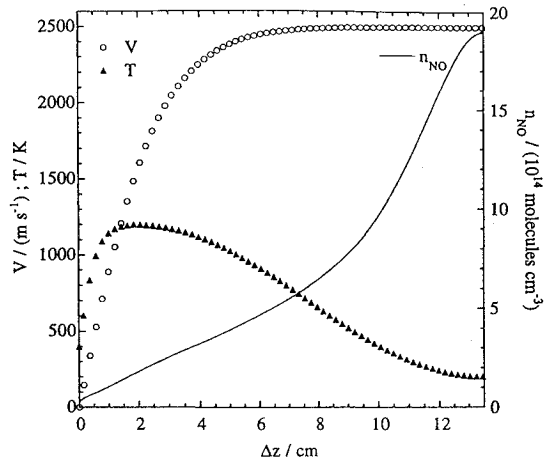

Fig. 3 Velocity, temperature, and NO concentration profiles used in the simulation of the effects of the boundary layers. Conditions are defined in Table 1.

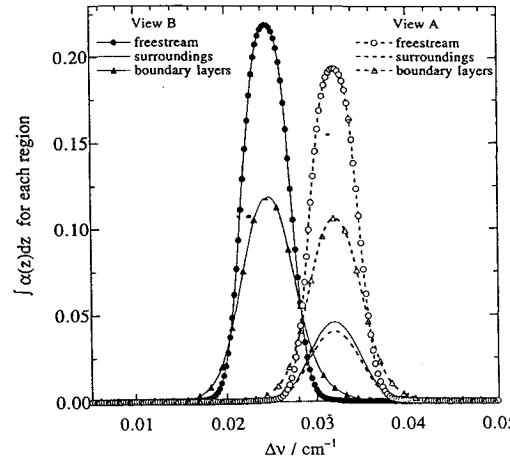

Fig. 4 Contribution of each region to the absorption around 1924.5 cm^{-1} for the conditions of Table 1 and for the boundary-layer profiles shown in Fig. 3.

Synthetic data were generated by computing transmission spectra through a flow to examine the effect of the neglect of the boundary layers in the analysis, as well as to test the fitting procedure in general. The beam path was broken into three regions for the simulation: 1) a path 40 cm long through a uniform core, 2) a path 233 cm long through a uniform external region, and 3) a boundary-layer region 27 cm long (2×13.5 cm) with variable properties. The boundary layers on either side of the flow are assumed to be identical for both views; i.e., axial variations of the boundary layer were neglected for view *B*. Hence, for each view, the boundary layer was replaced by a single region of the same total length when determining the influence on line-of-sight absorption. The velocity, temperature, and NO concentration profiles in the boundary were chosen to approximate the results of numerical simulations of laminar flow through the hypersonic nozzle,[7] while matching the values assumed for regions 1 and 2 on either end. Random noise of any desired amplitude and baseline slope and offset could be added to the simulated data to give a better simulation of experimental data. The simulated data were then analyzed by the same program used for the experimental data. The flow parameters deduced from the analysis could then be compared with the known inputs to estimate the influence of boundary-layer distortions and the sensitivity to noise and interference of the type seen in the experimental data.

Figure 3 shows boundary-layer profiles used in a typical simulation, and Table 1 lists the parameters used. The contributions of each region to the total absorption coefficient for each view are shown in Fig. 4. The figure shows that the boundary-layer contribution in view *B* is broad and somewhat asymmetric but has a peak that coincides with the absorption from the freestream. Figure 5 shows the

Table 1 Parameters for synthetic spectrum in F4[a]

	Path 1 (freestream)	Path 2 (surroundings)	Path 3 (boundary layers)
T/K	200	400	Variable
$n_{NO}/10^{14}$ molecule/cm^{-3}	19.0	0.253	Variable
Path length, L/cm	40	233	27
$n_{NO}L/10^{16}$ molecule/cm^{-2}	7.60	0.59	47.8
	View A (normal)		View B (biased at 63 deg)
Baseline offset	1.0×10^{-2}		-5.0×10^{-3}
Baseline slope	2.54×10^{-1}/cm^{-1}		1.27×10^{-1}/cm^{-1}

[a]Random noise amplitude, 0.5% of peak; 256 data points in each view; freestream velocity, 2500 m/s.

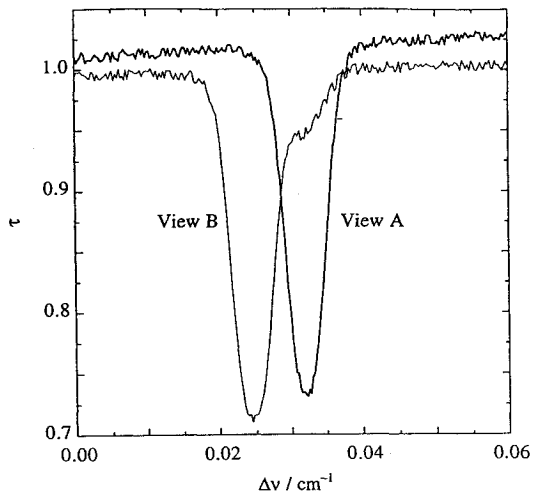

Fig. 5 Simulated experimental spectra for the conditions defined in Table 1 and the boundary-layer profiles shown in Fig. 3.

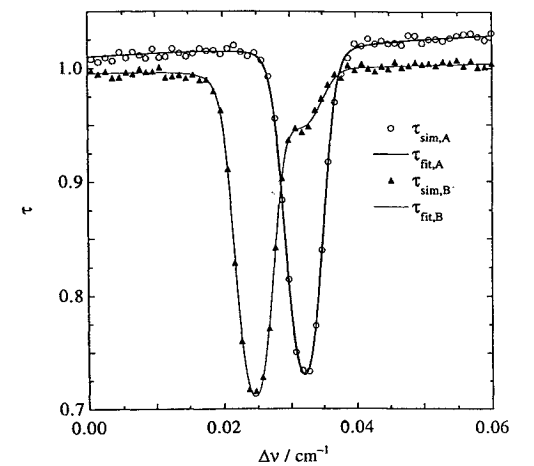

Fig. 6 Least-squares fit of model spectrum to simulated experimental spectra shown in Fig. 5. Only every fourth data point is shown for clarity.

corresponding simulated transmission record. It should be compared with the experimental records shown in Fig. 2. (Figure 8 shows the $t = 36$ ms record on a scale comparable to Fig. 5.)

Figure 6 shows the model spectra that provided a best fit to the synthesized records; only 25% of the synthesized data points are shown so that the fitted curves can be seen more clearly. The residual errors for each view are shown in Fig. 7. There are almost no detectable systematic errors because of the errors in the fitted temperature and neglect of boundary-layer distortion; they are masked by the random noise of 0.5% that was used when generating the synthetic transmission records. Table 2 summarizes the results of the fit. It can be seen that the velocity is accurately determined (error less than 1%), but there are significant discrepancies in the inferred

Table 2 Parameters for fitted spectrum with boundary layers not accounted for explicitly

	Path 1 (jet)	Path 2 (external region)
T/K	225	363
Error in T,%	+13	−9
$n_{NO}L/10^{16}$ molecule/cm^{-2}	9.7	0.64
$n_{NO}L/L =$ $n_{NO,eff}/10^{14}$ molecule/cm^{-3}	15	0.27
Error in $n_{NO,eff}$, %	−25	+9
	View A	View B
Baseline offset	0.96×10^{-2}	-5.70×10^{-3}
Baseline slope	2.60×10^{-1}/cm^{-1}	1.36×10^{-1}/cm^{-1}
Flow velocity, m/s	0	2483
Error in V, %	——	−0.7

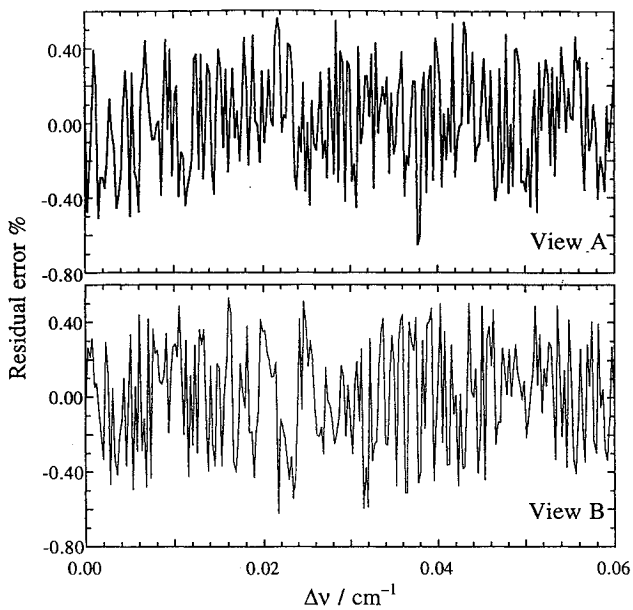

Fig. 7 Residual errors from least-squares fit to simulated data.

temperatures and integrated NO column densities. The percentage error in temperature is +12.5% for the flow if we attribute the results to the freestream; the corresponding error for the chamber is −9.1%. Errors of this magnitude are to be expected because of 1) the relatively weak dependence of Doppler broadening on temperature, 2) the coupling between Doppler and collision broadening in the Voigt line shape, and 3) distortions in the line shape arising from the boundary-layer absorption. The temperature determination is particularly sensitive to noisy data. It should be noted that higher spectral resolution in the profiles, i.e., higher speed digitization of the data during an experiment, would not improve definition of the line shape at the prevailing noise levels nor eliminate distortions due to boundary layers. Hence this would not improve the determination of the temperature if the same data analysis procedure were used.

The NO column density inferred depends on the fitted temperature through the integrated line intensity and hence is also subject to large uncertainties. The results obtained clearly do not correspond to the true integrated NO column density through flow and boundary layers. The boundary layers are highly inhomogeneous with strong variations in NO density and temperature (and hence line intensity). The line-of-sight average of these quantities makes a significant contribution to the integrated absorption, as shown in Fig. 4. If as a crude approximation we attempt to correct for the boundary-layer contribution to the core absorption by dividing the integrated column density by the total optical path in the flow (67 cm), then we obtain an estimate of 1.5×10^{15} molecules/cm^3 for the core. This is only 25% less than the assumed number density of 1.9×10^{15} molecules/cm^3 in the core for this particular case. In general, one should expect estimates no better than an order of magnitude. However, even such

rough estimates can be useful. It must be noted that the results given above are illustrative but not conclusive because of the approximate nature of the boundary-layer simulation.

Results and Discussion

Figure 8 shows the data records at $t = 36$ ms on a larger scale. Channel B is noisier because this channel had lower laser power levels. The corresponding fit is shown in Fig. 9; again only 25% of the data points are plotted so that one can more clearly see the lines representing the fitted transmission spectra. Although the fit misses the magnitude of the peak absorption in channel B, the doublet is correctly located and can be used to calculate the freestream velocity. Figure 10 shows the residual errors in the fits. The residual errors are not completely random, indicating systematic deviations from the model. These are to be expected in view of the neglect of boundary-layer distortions. However, the maximum error magnitudes are comparable to the noise levels in the data. The freestream velocity calculated from the fit is 2690 m/s. The static temperatures of NO inferred from the fit were 168 K for the flow and 634 K for the chamber. The NO column densities for the flow and chamber inferred from the fit were 3.4×10^{17} molecule/cm^2 and 2.1×10^{16} molecule/cm^2, respectively. The preceding simulation results show that these values are not very reliable because of the influence of the boundary layers that are neglected in the analysis.

Figures 11–14 summarize the results obtained when analyzing all data sets obtained in the tunnel run. Three of the 30 data sets were discarded because of data dropout during the scan—possibly due to particles passing through the laser beam. The variation of velocity with time is shown in Fig. 11. The average of all measurements is 2740 m/s with a standard deviation of 128 m/s (4.8%). However,

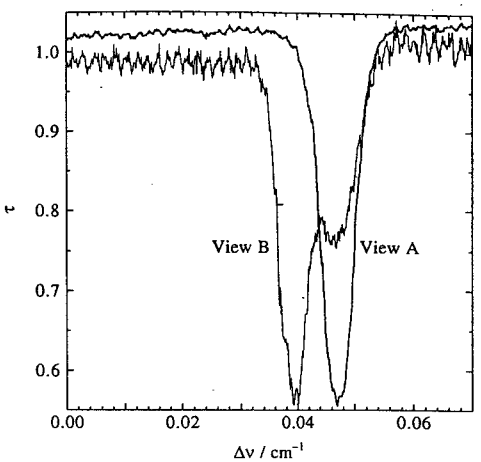

Fig. 8 Experimental data obtained at t = 36 ms shown on an expanded scale.

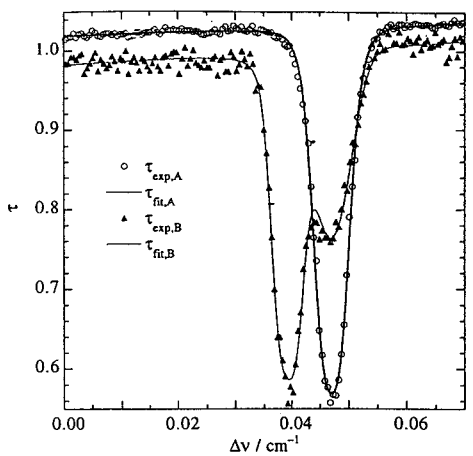

Fig. 9 Least-squares fit to the data shown in Fig. 8. Only every fourth data point is shown for clarity.

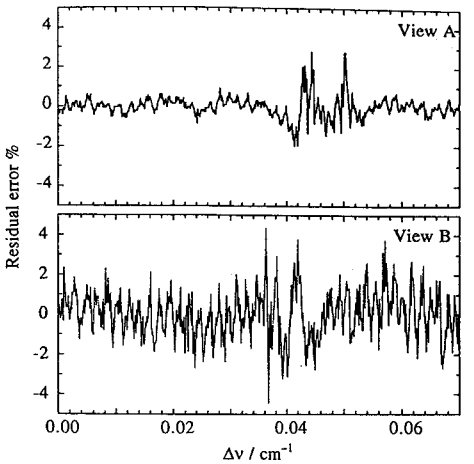

Fig. 10 Residual errors from the least-squares fit shown in Fig. 9.

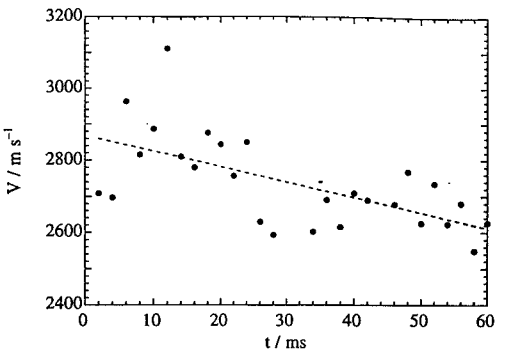

Fig. 11 Variation of freestream velocity in F4 as a function of time determined from the Doppler shift. The dashed line is a linear fit to the data to show the general trend in the data.

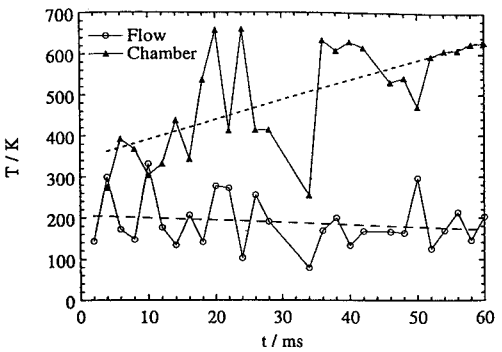

Fig. 12 Inferred variation of static temperature of the flow and the test chamber. The dashed lines are linear fits to the data to indicate trends.

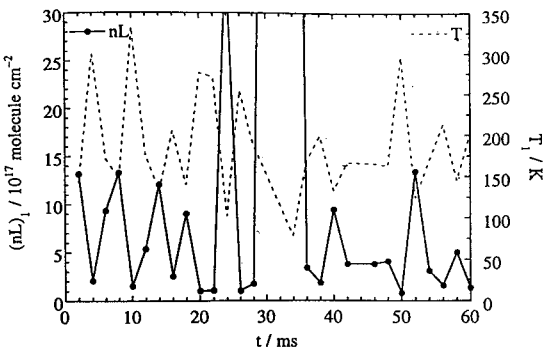

Fig. 13 Inferred variation of NO column density in the flow. The inferred static temperature is also displayed to show the inverse correlation induced by the analysis technique.

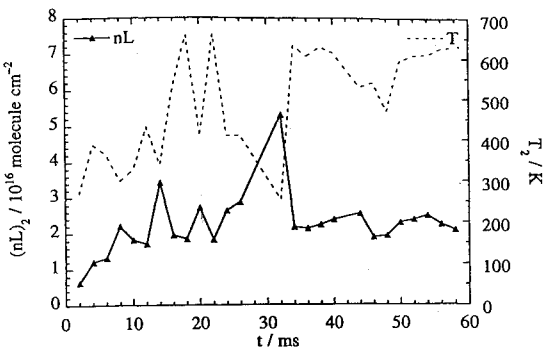

Fig. 14 Inferred variation of NO column density in the chamber. The inferred static temperature is also displayed to show the inverse correlation induced by the analysis technique.

some of this variation is systematic. The dashed line is a linear fit to the data and shows a decline of about 10% in flow velocity over the 60 ms duration of the run. This velocity evolution closely follows that obtained from flux probes that were also present during the experiment. The estimated uncertainty in the velocity measurement is ±5%. The largest contribution (±3.5%) to this uncertainty is in the measurement of the laser beam angle (±1 deg) relative to the flow, with smaller contributions from errors in the mean doublet positions determined by the fit model (±2%), uncertainty in the free spectral range of the etalon (±2%), and distortion of the doublet profiles due to the jet boundary layers (±2%).

The inferred static temperatures in the flow and the chamber are shown in Fig. 12. These show substantially greater variability, as might be expected in view of the comments made in the analysis section. The mean temperature in the flow is 188 K with a standard deviation of 64 K (35%). Because of the large fluctuations, the median value of 168 K is probably a better estimate of the flow temperature. The simulation results described before indicate that the true freestream temperature may be lower. The dashed line is a linear fit and shows that the temperature is effectively constant to within the measurement precision. Despite substantial variability in the fitted values, there appears to be a definite upward trend in the static temperature of the NO in the chamber during the experiment. This is consistent with the accumulation of hot gases not completely collected by the diffuser. The temperature rises from about 350 K at the beginning to 600 K at the end of the run.

The NO column densities inferred from the fits are strongly inversely correlated to temperature because of the dependence of doublet intensity on temperature [Eq. (5)]. This is seen in Figs. 13 and 14. Figure 13 shows that the inferred NO density is unrealistically high in those cases where the fitted freestream temperature approaches 100 K because the doublet intensity drops exponentially near this temperature. Using the median as a simple method to discard outliers, the column density of NO in the flow is about 4×10^{17} molecule/cm^2. This corresponds to a freestream NO density of approximately 5×10^{15} molecule/cm^3. The NO column density in the chamber plotted in Fig. 14 shows less variability because the line intensity is a weaker function of T at higher temperatures. The mean value is 2.2×10^{16} molecule/cm^2 with a standard deviation of 0.83×10^{16} molecule/cm^2. If the outliers are discarded, there is evidence on Fig. 14 of an initial rise and then a relatively constant value. The corresponding chamber NO density is 9×10^{13} molecule/cm^3 with an estimated uncertainty of ±20%.

One of the sources of the wide variability in the inferred temperature is the least-squares fitting procedure itself. It is well known that least-squares procedures are sensitive to outliers in the data. This has a particularly strong influence on the temperature and, consequently, on the NO concentration. The present data records are relatively noisy, and it is likely that most experiments in the hypersonic tunnel will have significant interferences. Hence, a non-least-squares fitting algorithm that would be much more stable than the present procedure is very desirable. A different NO transition, whose integrated intensity is less sensitive to temperature over the temperature range, might also give better results. One problem with finding such a transition is the very wide temperature range encountered in these experiments; the freestream is cold, and there are very hot regions in the boundary layers. The optimal transition will have to be determined by detailed analyses of simulated spectra of the type described earlier.

Conclusions

Diode laser absorption of NO has proved to be a useful diagnostic for nonintrusive velocity measurements in F4. The velocity measurements were not affected by the boundary layers for the spectral transition chosen. However, absorption in the boundary layers leads to significant systematic errors in the inferred temperature and consequently the NO density because it distorts the line profile. This distortion affects the inferred Doppler width, which is inherently relatively insensitive to temperature. Improved temperature measurements would be obtained by scanning the laser over two closely spaced transitions arising from different rotational states. If a suitable pair is not available, two independent laser beams could be used to probe different rotational states. The laser beams can be combined and then separated using orthogonal polarizations. Of course, this would increase the cost of the experimental setup.

The present analysis gave the freestream temperature with an estimated precision of about 35% and order of magnitude estimates of NO densities. Because the experimental data are quite noisy, parameters inferred from the least-squares fit are adversely affected by outlying points. Future work will be directed to improving the analysis procedure by using non-least-squares fits. Such a procedure would make the multiple parameter fit more stable. Note that the advantage of non-least-squares procedures is that they are less sensitive to outliers; they will not eliminate the inherent insensitivity of line shape to temperature. We believe they will reduce the wide variance in inferred temperature and NO concentration because of the nonlinear coupling between fit parameters in the model. In future work we will assess the improvement in temperature estimates obtained using non-least-squares models to analyze these data. A two-line temperature determination with properly chosen spectral lines should provide a better estimate of temperature than the procedure used here. Non-least-squares fitting strategies would be very useful when analyzing such data records too, if they are noisy (as is likely).

Finally, a more sophisticated analysis that accounts for boundary-layer distortion needs to be developed. Because this requires the introduction of additional parameters in the fit, it can best be done after an improved fitting algorithm is developed.

Acknowledgments

The experimental work was supported by a contract from Dassault Aviation. The data presented in this paper correspond to run No. 523 of the F4 facility. The last author gratefully acknowledges a Senior Scholar Award from the Fulbright Foundation in fall 1993 and support from ONERA, the National Science Foundation, and the University of Texas at Austin.

References

[1]Masson, A., "Qualification de l'écoulement dans la Soufflerie F4," PV Onera, No. 1/8687 GY, 1993, ONERA, Chatillon, France, 1993.

[2]Bugeau, A., and Castan, E., "Hermes First Force Measurement in ONERA-F4 Wind Tunnel," *Proceedings: Second European Symposium on Aerothermodynamics for Space Vehicles and Fourth European High-Velocity Data Base Workshop*, edited by J. J. Hunt, European Space Agency SP-367, European Space Research and Technology Center, Noordwijk, The Netherlands, 1994, pp. 229–236.

[3]Amiot, C., Bacis, R., and Guelachvili, G., "Infrared Study of the $X^2\Pi v = 0, 1, 2$ Levels of $^{14}N^{16}O$. Preliminary Results on the $v = 0, 1$ Levels of $^{14}N^{17}O$, $^{14}N^{18}O$, and $^{15}N^{16}O$," *Canadian Journal of Physics*, Vol. 56, No. 2, 1978, pp. 251–265.

[4]Amiot, C., "The Infrared Emission Spectrum of NO: Analysis of the $\Delta v = 3$ Sequence up to $v = 22$," *Journal of Molecular Spectroscopy*, Vol. 94, No. 1, 1982, pp. 150–172.

[5]Ouyang, X., and Varghese, P. L., "Reliable and Efficient Program for Fitting Galatry and Voigt Profiles to Spectral Data on Multiple Lines," *Applied Optics*, Vol. 28, No. 8, 1989, pp. 1538–1545.

[6]Garbow, B. C., Hillstrom, K. E., and More, J. J., *MINPACK Project*, Argonne National Lab., Argonne, IL, 1980.

[7]Masson, M., private communication, Aerospatiale, Paris, France, Nov. 1993 (similar results are presented in the Workshop of Ref. 2).